292 *Macromolecules* **2010**, *43*, 292–298
DOI: 10.1021/ma901980b

Macromolecules
ARTICLE

Anisotropic Proton Conduction in Aligned Block Copolymer Electrolyte Membranes at Equilibrium with Humid Air

Moon Jeong Park*,† and Nitash P. Balsara*,‡,§,∥

†*Department of Chemistry, Division of Advanced Materials Science, Pohang University of Science and Technology (POSTECH), Pohang, Korea 790-784,* ‡*Department of Chemical Engineering, University of California, Berkeley, California 94720,* §*Materials Sciences Division, and* ∥*Environmental Energy Technologies Division, Lawrence Berkeley National Laboratory, University of California, Berkeley, California 94720*

Received September 4, 2009; Revised Manuscript Received November 7, 2009

ABSTRACT: The effect of alignment of proton-conducting domains in hydrated poly(styrenesulfonate-*b*-methylbutylene) copolymer films on conductivity was studied by impedance spectroscopy. Pressing isotropic samples obtained by casting results in lamellae aligned in the plane of the film. Application of electric fields and flow fields on the isotropic samples results in lamellae aligned perpendicular to the plane of the film. The alignment of lamellae, quantified by a combination of two dimensional small angle X-ray scattering (SAXS), birefringence, and transmission electron microscopy (TEM), was much better in the pressed samples than in the field-aligned samples. Conductivity was measured in the plane of the film ($\sigma_{\parallel}$) and normal to the plane of the film ($\sigma_{\perp}$). Only the pressed sample showed highly anisotropic proton conduction with $\sigma_{\parallel}/\sigma_{\perp} = 75$. In this case, the value of $\sigma_{\parallel}$ increased by 30% after alignment, relative to that obtained from the as-cast samples. The values of $\sigma_{\parallel}/\sigma_{\perp}$ obtained after electric field and shear field alignment were 1.2 and 1.4, respectively, in spite of partial alignment of the domains, and the increase in $\sigma_{\perp}$ after alignment was less than 20%.

Introduction

Proton exchange membrane fuel cells offer the prospect of supplying clean electrical power for a wide variety of systems such as portable electronic devices and vehicles.[1−3] Polymer electrolyte membranes (PEMs) with hydrophilic, proton conducting channels embedded in a structurally sound hydrophobic matrix play a central role in the operation of fuel cells. Significant effort has been devoted to improvement of the transport properties of PEMs.[4−11] In most cases, the hydrophilic channels in PEMs are obtained by self-assembly, which, in the absence of external fields, leads to randomly oriented conducting domains. It is clear that aligning these domains perpendicular to the film will lead to improved conductivity.

We define $\sigma_{\parallel}$ and $\sigma_{\perp}$ to be the conductivities of PEMs in directions parallel and perpendicular to the plane of the film, σ_h and ϕ_h to be the intrinsic conductivity and volume fraction of the hydrophilic domains, respectively. If we assume that the conductivity of the hydrophobic phase is negligible, the maximum conductivity that can be obtained from a composite PEM is given by $\sigma_{max} = \sigma_h\phi_h$. We consider two extreme cases of alignment: (1) where the conducting domains are in the plane of the film, i.e., the parallel alignment and (2) where the conducting domains are perpendicular to the plane of the film, i.e., the perpendicular alignment. For the parallel orientation, we expect $\sigma_{\parallel} = \sigma_{max}$ and $\sigma_{\perp} = 0$, while for perpendicular orientation, we expect $\sigma_{\parallel} = 0$ and $\sigma_{\perp} = \sigma_{max}$. The simplest expression for the conductivity of a collection of randomly oriented isotropic grains is $\sigma_{iso} = \sigma_{\parallel} = \sigma_{\perp} = d\sigma_{max}$, where the constant d depends on the geometry of the conducting channels.[12−14] For cylindrical (1-dimensional) channels, $d = 1/3$, while for lamellar channels, $d = 2/3$. Our treatment of randomly oriented grains assumes connectivity across grain boundaries.

*Corresponding authors. E-mail: moonpark@postech.ac.kr (M.J.P.); nbalsara@berkeley.edu (N.P.B.).

The above arguments indicate that alignment would lead to extremely anisotropic conductivity values (e.g., $\sigma_{\perp}/\sigma_{\parallel} = \infty$ for perpendicular alignment). However the increase in conductivity along the aligned direction, σ_{align}, relative to the isotropic sample would be relatively modest, ranging from a factor of 3 in the case of cylindrical domains to 1.5 in the case of lamellar samples.

Experimental data obtained from PEMs are qualitatively different from the predictions given above. We are not aware of any study of unaligned PEMs where $\sigma_{iso} = \sigma_{\parallel} = \sigma_{\perp}$ has been observed. For the most widely studied case of Nafion, $\sigma_{\parallel}/\sigma_{\perp}$ values of about 3 are usually obtained.[15−17] The value of σ_{iso} is thus not well-defined even in this simple case. The effect of processing on alignment of the conducting channels and crystallinity of the matrix has been investigated using NMR and X-ray diffraction (XRD).[18−20] Stretching Nafion orients the conducting domains along the stretching direction. The value of $\sigma_{\parallel}$ increases by a factor of 1.4 after stretching.[20] The reason for this increase is not entirely clear as the morphology of Nafion in the unstretched state, in both dry and hydrated states, remains unresolved.[15−20] The morphology of PEMs based on block copolymers such as sulfonated poly(styrene-*b*-isobutylene-*b*-styrene) is clearly resolved, at least in the unaligned dry state.[15] In this case, $\sigma_{\parallel}/\sigma_{\perp}$ varies from 9 to 43 depending on the level of sulfonation. There is thus considerable ambiguity regarding the value of σ_{iso} in block copolymer PEMs. External fields such as large amplitude shear flow and tensile stress[21−23] were utilized to achieve the alignment of nanostructures in the block copolymer PEMs. For the case of poly(styrene)-*b*-poly(4-vinyl pyridine), a 60-fold increase in $\sigma_{\parallel}$ was obtained after alignment.[21]

Unfortunately the conductivity of PEMs through the films is most relevant for practical applications. The discussion above shows that in most cases, the measured conductivity in this direction lower than that along the film of the plane. This is because simple methods for processing thin films result in parallel alignment of the conducting domains. The application of electric

 Published on Web 12/02/2009

fields perpendicular to the films[24] and appropriate surface modification[25,26] results in perpendicular alignment of the conducting domains. Umeda et al. demonstrated that PEMs aligned under electric fields exhibited 10 times higher proton conductivity along normal to the plane than that prepared without the electric field.[24] Elabd et al. reported $\sigma_\perp$ values that were a factor of 6 higher than σ_{iso} using commercial polycarbonate track-etched membranes as templates for creating model PEMs with conducting domains in the perpendicular orientation.[26] There is clearly no consensus on the extent to which alignment leads to improved conductivity.

The purpose of this paper is to report on the effect of alignment on proton transport in hydrated block copolymer membranes. The system of interest is a nearly monodisperse poly(styrenesulfonate-*b*-methylbutylene) (PSS−PMB) copolymer with total molecular weight of 5.7 kg/mol. The volume fraction of the dry PSS microphase ϕ_{PSS}, is 0.465. This copolymer forms a lamellar phase in both the dry and hydrated states. The properties of unaligned PSS−PMB copolymers have been thoroughly investigated in previous papers.[27−31] We applied a variety of external fields to orient the conducting lamellae. Small angle X-ray scattering (SAXS), in situ birefringence, and transmission electron microscopy (TEM) were used to quantify the structural anisotropy thus generated. We present data on the effect of lamellar alignment on both in-plane and through-plane conductivity.

Experimental Section

Materials. A PS−PMB with PS and PMB molecular weights of 2.5 and 2.6 kg/mol, respectively, was synthesized by sequential anionic polymerization of styrene and isoprene followed by selective hydrogenation of the polydiene. The polydispersity index of the copolymer was 1.02. The sample studied here is called P3(21) where 3 indicates the nominal molecular weights of the blocks in kg/mol and 21 signifies that 20 mol% of the PSS block is sulfonated. The PS blocks of the PS−PMB copolymer were then partially sulfonated using procedures described in ref 32. Assuming that the sulfonation reaction rate is independent of local environment, we expect the PSS block to be a random copolymer of sulfonated and unsulfonated segments. Details concerning the synthesis procedures used are given in our recent publications.[29] P3(21) films with thicknesses ranging from 180 to 220 μm were prepared by solvent casting using THF as a solvent under a nitrogen blanket for 2 days followed by vacuum drying at 50 °C for 10 days. Free standing films were obtained by carefully peeling off the sample from a polyimide substrate using a sharp surgical knife. We refer to these as as-cast films. The as-cast films were subjected to three alignment protocols to give three different kinds of aligned films.

(*1*) *Pressed Films*. The as-cast film was subjected to a normal stress of about 200 kgf/cm^2 in a hydraulic Carver press at 21 °C for 12 h in dry air. This resulted in a decrease in the sample thickness (e.g., 220 to 190 μm) while the sample diameter increased by about 5−10%. We refer to these as the pressed samples.

(*2*) *Films Aligned by an Electric Field*. As-cast P3(21) films were placed between two conducting indium−tin−oxide (ITO) coated glass (3 cm × 5 cm) plates. A dc electric field (E-field) between 5 and 15 kV/cm was applied using a Keithley power supply. A 2.0 mm air gap was present between the top ITO coated glass and P3(21) film. The electrode and film assembly was placed in a home-built aluminum sample chamber equipped with two quartz windows to allow transmission of a laser beam through the sample. Water from a well located within the sample chamber was used to humidify the air surrounding the sample, which yielded a stable RH of 97%. The samples were equilibrated for 2 days within the sample chamber before the alignment experiments. The absorption of water in the sample lowers the glass transition temperature (Tg) of the PSS-rich microphase (Tg of the hydrophobic PMB-rich microphase is lower than room temperature) and enables alignment at room temperature. In addition, hydration increases the difference in dielectric constants between hydrated PSS and hydrophobic PMB domains.

In situ birefringence measurements were conducted on the P3(21) sample using an apparatus described in ref 33. The Nd:YAG laser beam (wavelength, λ = 532 nm) was directed through the samples held between two crossed polarizers. We studied the effect of the applied E-field on alignment by orienting the incident beam at an angle θ = 45° relative to the axis of the instrument and recording the birefringence signal $I(45°)$ normalized by the incident beam intensity, I_0. The increase in time-dependent intensity $I(45°)$ indicates the formation of perpendicular lamellae. After the E-field alignment was completed, the polarizer and analyzer were rotated relative to the axis of the instrument to record $I(\theta)$ at θ values other than 45°.

(*3*) *Films Aligned by a Shear Flow Field*. The as-cast sample was placed in a parallel plate shear cell described in refs 33 and 34. As was the case with the electric field experiments, the film was first exposed to air with RH = 97% and T = 21 °C for 2 days and then exposed to reciprocating shear flow with a frequency of 0.1 Hz and a strain amplitude of 250% at the same RH and T conditions. The top plate was translated using a computer-controlled motor, and the bottom plate was stationary. As was the case with the E-field experiments, we studied the effect of flow on alignment by orienting the incident beam at an angle θ = 45° relative to the axis of the flow direction and recording the birefringence signal $I(45°)$ normalized by I_0.

For the alignment studies with solvent casting, pressure, and E-field, five independent samples were prepared for each method. In the case of shear-aligned samples, only data obtained from the best aligned sample is discussed due to experimental problems in preparing the samples. In the later case, the sample was cut into 2 pieces and analyzed for alignment and conductivity. Similar results were obtained from both pieces.

Small Angle X-ray Scattering. Synchrotron SAXS measurements on the aligned P3(21) sample in the dry state were carried out at the beamline 7.3.3 equipped with a CCD detector (2304 × 2304 pixels) at the Advanced Light Source (ALS), Lawrence Berkeley National Laboratory (LBNL). The wavelength of the incident X-ray beam was 0.15 nm ($\Delta\lambda/\lambda = 10^{-4}$), and the sample-to-detector distance of 2.0 m was used yielding scattering wave vector q ($q = 4\pi \sin(\theta/2)/\lambda$, where θ is the scattering angle) in the range 0.1−2.5 nm^{-1}. The resulting two-dimensional scattering data were averaged azimuthally to obtain intensity versus q. The scattering data were corrected for the CCD dark current and the scattering from air and Kapton windows.

Transmission Electron Microscopy (TEM). The aligned P3(21) samples were cryo-microtomed at −100 °C to obtain thin sections with thicknesses in the 50−80 nm range using an RMC Boeckeler PT XL Ultramicrotome. The electron contrast in the P3(21) samples was enhanced by exposure to ruthenium tetroxide (RuO_4) vapor for 50 min, which preferentially stains the PSS phase. Imaging of stained samples was performed with a Zeiss LIBRA 200FE microscope operating at 200 kV equipped with a cold stage (−160 °C) and an Omega energy filter. Images were recorded on a Gatan 2048 × 2048 pixel CCD camera (Gatan Inc., Pleasanton, CA). All data sets were acquired using Digital Micrograph (Gatan, Inc.) software.

Conductivity Measurements. Proton conductivity of P3(21) samples described above were measured using ac impedance spectroscopy. The aligned P3(21) samples were located within the humidity chamber under the saturated water vapor (RH = 98%), and the proton conductivity was measured every 30 min until steady values were obtained. The in-plane conductivity, $\sigma_\parallel$, was measured using a four-electrode probe (BekkTech LLC, Loveland, CO) as shown schematically in Figure 1a. The probe consisted of a Teflon block, a membrane clamp, two platinum gauzes, and two platinum wires. The two platinum wires were used as working and counter electrodes to apply a current to the sample membrane (2.0 cm × 1.0 cm, 220 μm thick) through the two platinum gauzes, and the two platinum wires 0.425 cm apart

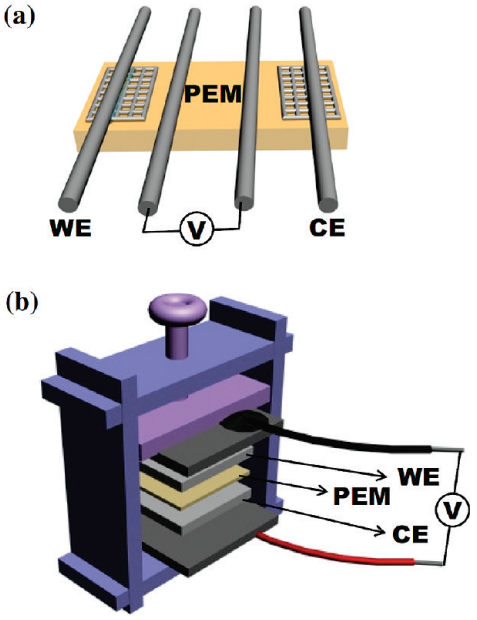

Figure 1. Conductivity cells with (a) a four-electrode probe to measure $\sigma_{\parallel}$ and (b) a two-electrode cell probe to measure $\sigma_{\perp}$. WE and CE represent the working electrode and counter electrode, respectively.

were used as reference electrodes. The normal-to-plane conductivity, $\sigma_{\perp}$, was measured using a home-built two-electrode cell with 1.25 cm × 1.25 cm two stainless steel blocking electrodes, and 1 cm × 1 cm Pt working/counter electrodes as shown in Figure 1b. The 1.0 cm × 1.0 cm P3(21) sample (220 μm thick) was placed in between Pt electrodes at a constant pressure of 1.2 kgf/cm^2 for accurate impedance measurements. The aligned samples were dipped in deionized water, placed quickly between the electrodes, and placed in the humidity chamber. Data were taken until the measured conductivity reached a plateau. This was necessary because of the limited contact between air and the sample in this geometry. Both $\sigma_{\parallel}$ and $\sigma_{\perp}$ were measured using a Gammry potentiostat operating over a frequency range of 1−100 000 Hz.

Results

Two-dimensional SAXS patterns obtained by directing the X-ray beam through the films prepared by the procedures described above and schematic drawings of the resulting lamellar orientations are shown in Figure 2. The SAXS signal mainly reflects the subset of grains with lamellar normals oriented perpendicular to the direction of the incident beam, i.e., lamellae with normals parallel to the plane of the film. The SAXS pattern of the as-cast sample consists of an isotropic ring consistent with a random orientation of grains (Figure 2a). In contrast, the pressed sample exhibits a much weaker isotropic ring indicating the predominance of lamellar normals aligned out of the plane of the film (Figure 2b). Following literature, we refer to this as the parallel orientation.[35,36] The SAXS pattern from the sample aligned using the electric-field (15 kV/cm E-field) exhibits a sharp isotropic ring with six spots superposed on the ring (Figure 2c). This indicates the dominance of lamellae with perpendicular alignment.[37−40] It is interesting to note that these six-spot patterns were always observed after E-field alignment although the relative intensity and position of SAXS peaks varied from run to run. The four dominant spots (among six spots) in the SAXS pattern indicate the two dominant directions for orientation of the lamellar normals while the presence of the ring suggests that these lamellae coexist with randomly oriented grains. The SAXS pattern from the sample aligned using shear flow exhibits two arcs (Figure 2d). This indicates one dominant orientation of

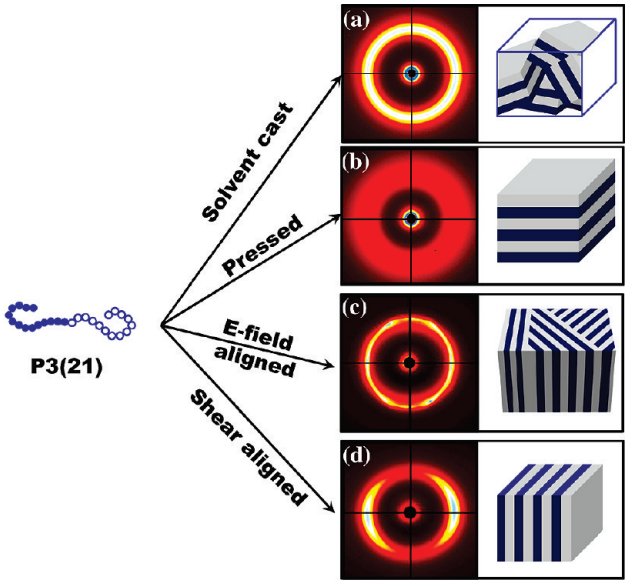

Figure 2. 2D SAXS patterns and schematic views of domain orientation of films prepared by methods as indicated.

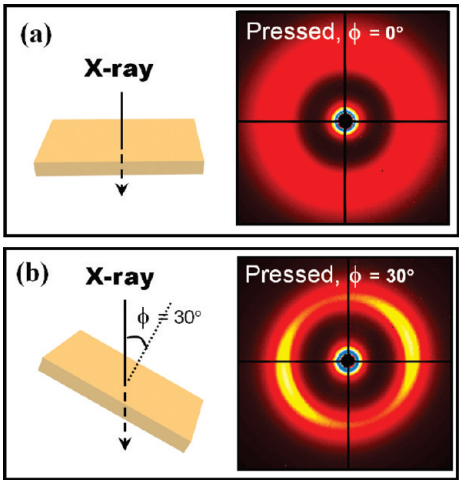

Figure 3. 2D SAXS patterns obtained from the pressed sample at tilting angles (ϕ) of (a) 0° and (b) 30°.

lamellar normals. While both E-fields and shear flow create lamellae with the same general alignment, the E-field is isotropic in the plane of the film and thus there is no preferred orientation of the lamellae. In contrast, the direction of flow provides a natural alignment direction for the perpendicular lamellae.[35,41−45] The SAXS profile of the pressed film was recorded as a function of tilt angle (ϕ), and the results are shown in Figure 3. The SAXS data at ϕ = 30° shows strong arcs, confirming the presence of parallel lamellae. This rules out the possibility that the weak scattering ring at ϕ = 0° is due to disordering of the sample.

For the case of shear alignment and E-field alignment, the change in domain orientation during the alignment process is monitored by birefringence measurements. Figure 4a shows plots of $I(45°)/I_0$ versus time for the shear alignment protocol. The increase in $I(45°)/I_0$ by about an order of magnitude and the corresponding SAXS data [also shown in Figure 4a] unambiguously indicate the formation of perpendicular lamellae under the shear flow field. The time to complete the lamellar alignment process was approximately 1 h. Changing the flow parameters did not result in any qualitative change in lamellar orientation. Figure 4b shows plots of $I(45°)/I_0$ versus time for two E-field alignment protocols.

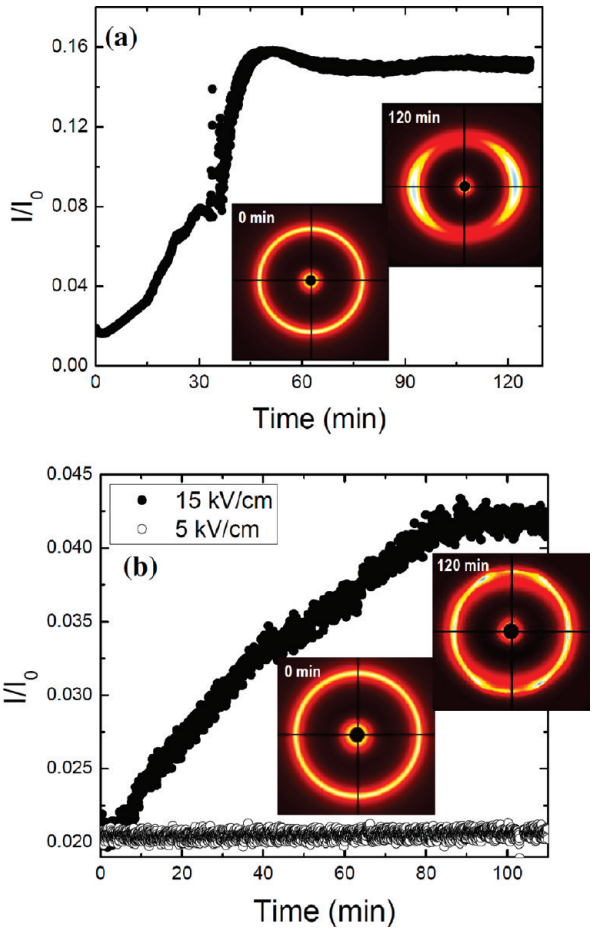

Figure 4. In situ birefringence measurements as a function of time during (a) shear flow alignment and (b) E-field alignment. The inset figures show 2D SAXS patterns obtained at different times.

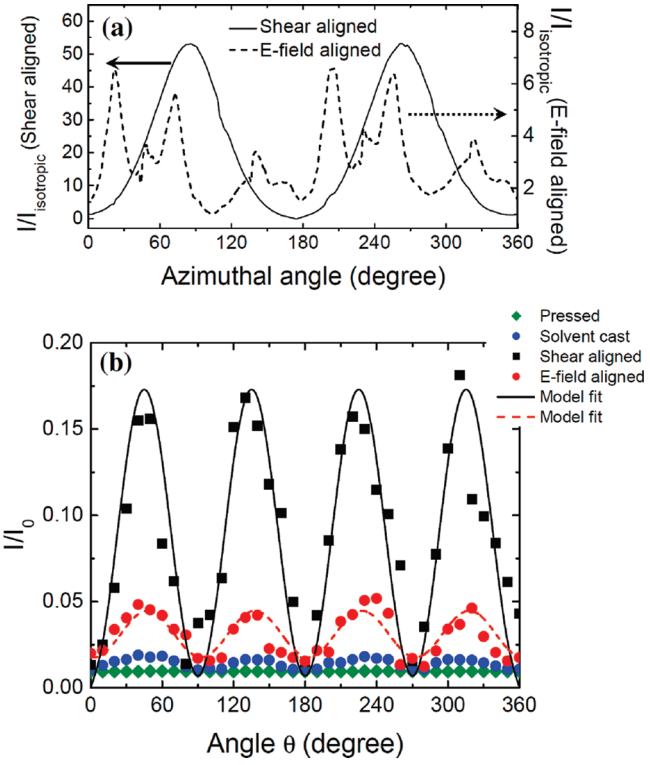

Figure 5. (a) Azimuthal scans of the 2D SAXS patterns of shear flow aligned and E-field aligned samples. The SAXS intensities of the aligned samples are normalized by those of the isotropic sample prior to alignment. (b) Dependence of the birefringence signal, I/I_0, on angle θ. For the shear flow aligned sample, θ is the angle between the polarizer orientation and the flow direction. Data from other samples were shifted along the θ axis to match the peak locations at $\theta = 45°$.

The application of $E = 15$ kV/cm results in an increase in I/I_0, while the application of $E = 5$ kV/cm does not. Not surprisingly, there is a threshold for E-field alignment. The magnitude of $I(45°)/I_0$ upon completion of the E-field alignment is significantly lower than that of the shear flow alignment (compare parts a and b of Figure 4) indicating that the E-field results in poorer alignment when compared to the flow field. While all of the as cast samples showed isotropic SAXS rings, there was some variability in the patterns obtained as seen in the $t = 0$ data for the E-field and shear samples (parts a and b of Figure 4). The shear flow data are more scattered than the E-field data (compare parts a and b of Figure 4). We suspect that this is due to the motion of one of the optical windows and the fact that different portions of the samples are in the beam at different times in the shear flow experiment.

The SAXS intensity in the range $0.5\ \text{nm}^{-1} < q < 1.1\ \text{nm}^{-1}$ was computed as a function of azimuthal angle of shear aligned P3(21) and E-field aligned P3(21), obtained after completion of the alignment process (i.e., after 2 h) and the results, after normalization of the signal obtained from the as-cast samples, are given Figure 5a. The multiple peaks in the E-field aligned sample indicate the lack of a preferred orientation direction for the perpendicular alignment while the two peaks in the shear flow aligned sample indicate the presence of a preferred orientation direction. The normalized intensity of shear aligned sample is a factor of 7 larger than that of E-field aligned sample. This is another measure of the fact that our best perpendicular alignment is obtained under shear flow.

After completion of the alignment under E-field and shear flow protocols, the aligned samples were dried in a vacuum oven for 5 days at room temperature. The dried free-standing P3(21) samples were then placed back in the birefringence apparatus and $I(\theta)/I_0$ was measured as a function of θ by manually rotating the crossed polarizers. In Figure 5b, we compare $I(\theta)/I_0$ for the dry as-cast, pressed, and aligned films. The theoretical expression of $I(\theta)/I_0$ for a single grain of perpendicular lamellae is[46−48]

$$\frac{I}{I_0} = \sin^2 2\theta \sin^2\left(\frac{\pi}{\lambda}\Delta n l_{\text{ave}}\right) \qquad (1)$$

where Δn is the difference between the refractive indices for light polarized parallel and perpendicular to the lamellae, l_{ave} is average length of the grain in the light propagation direction, and λ is the wavelength of the incident beam. Modulations consistent with eq 1 were observed in all of the aligned samples. θ for the flow and E-field aligned samples was defined so that the peaks in $I(\theta)/I_0$ were obtained at values consistent with eq 1. $I(\theta = 45°)/I_0$ of the aligned samples were not significantly altered by drying (compare peaks in Figure 5b with the long time data in Figure 4). It is evident that the alignment obtained under E-fields and shear flow is not altered when the samples are removed from the humid environment. The magnitude of the oscillating birefringence signal can be taken as an indication of the extent of alignment of the perpendicular lamellae. The $I(\theta)/I_0$ profile of the as-cast sample exhibits mild oscillations, suggesting a slightly nonrandom grain orientation. The development of such anisotropy has been seen in previous studies of solvent-cast block copolymers.[15,49−51] The $I(\theta)/I_0$ profile of the pressed sample has significantly smaller oscillations. This is mainly due to the fact that most of the lamellae are in the parallel orientation and they do not contribute to $I(\theta)/I_0$. Significant oscillations in the $I(\theta)/I_0$ profiles are seen in the E-field and flow aligned samples (Figure 5b). The solid curve through the shear flow data set in

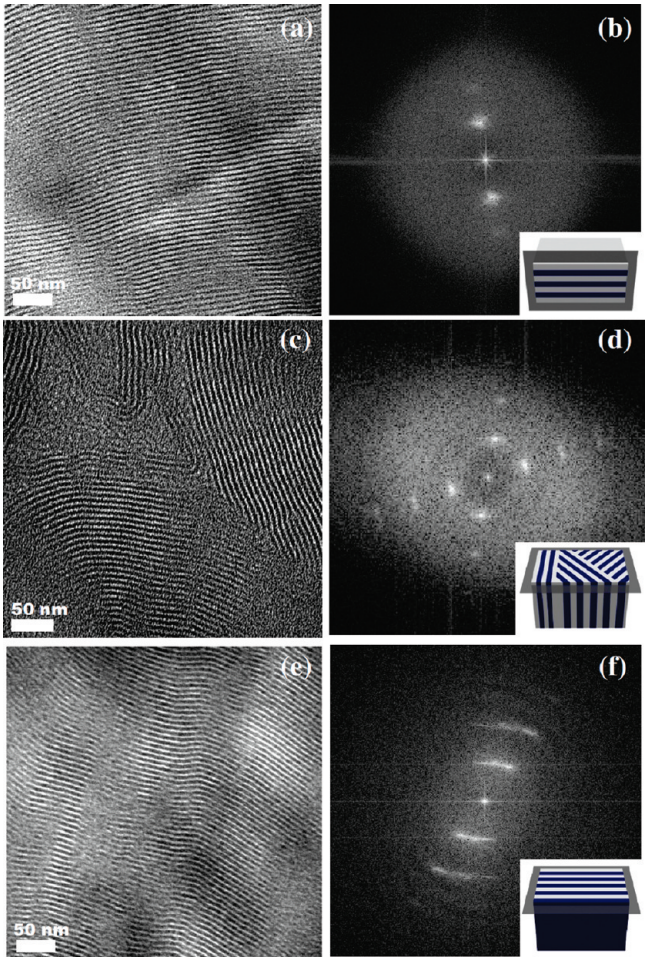

Figure 6. Cross-sectional TEM images and FFT patterns of (a, b) pressed films, (c, d) films aligned by E-field, and (e, f) films aligned by shear flow. The PSS domains were darkened by RuO_4 staining. The graphics in the FFT patterns illustrate the direction of cross-sectioning of aligned samples.

Figure 5b represents least-squares fits of eq 1 with Δnl_{ave} as the only adjustable parameter. If we assume that the argument of the second sin term in eq 1 is less than $\pi/2$, then the product Δnl_{ave} reflects the properties of the aligned grain which is assumed to be a "single-crystal". In contrast, since the SAXS data indicate that the E-field aligned sample shows multiple perpendicular grain orientations, we use the following expression for $I(\theta)/I_0$

$$\frac{I}{I_0} = \sin^2 2\theta \sin^2\left(\frac{\pi}{\lambda}\Delta nl_{ave}\right) + \sin^2 2(\theta+51°)\sin^2\left(\frac{\pi}{\lambda}\Delta n(1.1l_{ave})\right) + \sin^2 2(\theta+61°)\sin^2\left(\frac{\pi}{\lambda}\Delta n(0.9l_{ave})\right) \quad (2)$$

where the angles in the first sin term of each product in eq 2 were determined from the azimuthal SAXS profile (Figure 5a). The prefactors 1.1 and 0.9 in the second sin term of each product, which reflect relative grain sizes of lamellar domains at each orientation angle, was obtained by integrating the areas under the peaks in the azimuthal SAXS profile in Figure 5a. The model fit, shown by the dashed curve in Figure 5b, provides an estimate of Δnl_{ave}. The fitted value of Δnl_{ave} for the flow aligned sample is a factor of 5 larger than that of the E-field aligned sample. The value of the ratio of Δnl_{ave} obtained from the best shear-aligned sample and five different E-field aligned samples is 4.3 ± 0.7 to 1. This indicates that the characteristic length of the E-field aligned crystals is a factor of 4−5 smaller than the single crystal obtained under flow. The data in Figure 5b thus provide additional quantification of the differences in alignment obtained by the different processes employed in this study.

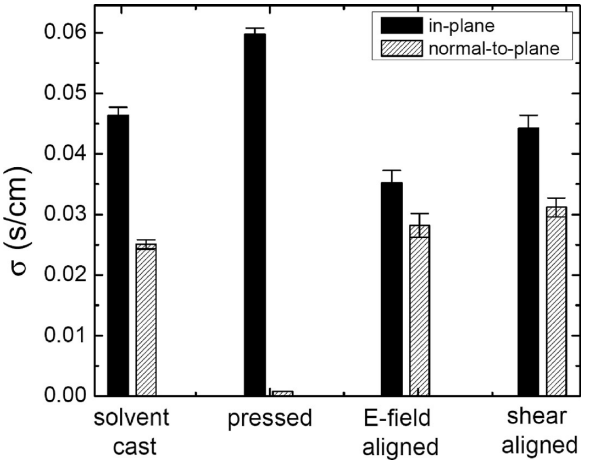

Figure 7. The equilibrium in-plane and normal-to-plane conductivity values of as-cast and aligned samples.

To further elucidate the nature of the aligned lamellar structure of P3(21) samples, the morphology of each sample is examined by TEM. Samples were cross-sectioned along either in-plane (E-field and flow field) or normal-to-plane (pressed film) directions. In Figure 6, we show typical TEM images and corresponding FFT patterns obtained from the pressed sample (parts a and b), E-field alignment (parts c and d), and shear alignment (parts e and f). The sectioning direction is indicated by a graphic inset for each processing condition. The best alignment was seen in both position and reciprocal data obtained from the pressed sample (parts a and b of Figure 6). Coexistence of differently oriented grains was seen after E-field alignment (parts c and d of Figure 6). The ordered lamellae of the flow aligned sample (parts e and f of Figure 6) exhibited a wavy texture resulting in arcs in the fast Fourier transform (FFT) that are similar to the arcs seen in the SAXS patterns (Figure 4a). We obtained specimens from different locations within the films up to a depth of about 100 μm from the top surface and found no significant difference in the micrographs.

We now discuss the effect of domain alignment on proton conductivities, $\sigma_\parallel$ and $\sigma_\perp$. The samples were equilibrated at RH = 98% and T = 25 °C, and the proton conductivity was measured every 30 min to track humidification kinetics. For all cases, the proton conductivity is reported after 4 days to minimize non-equilibrium effects. Note that SAXS, birefringence, TEM, and conductivity measurements were conducted on the same sample. We first measured $\sigma_\parallel$ and $\sigma_\perp$ of Nafion 117 and obtained $\sigma_\parallel$ = 0.077 S/cm and $\sigma_\perp$ = 0.025 S/cm ($\sigma_\parallel/\sigma_\perp = 3.1 \pm 0.3$). This result is in good agreement with results reported by other groups, $\sigma_\parallel$ = 0.067 $\sigma_\perp$ = 0.027 S/cm,[15] $\sigma_\parallel$ = 0.067 and $\sigma_\perp$ = 0.024 S/cm,[16] $\sigma_\perp$ = 0.022 S/cm.[17] The lack of equality of $\sigma_\parallel$ and $\sigma_\perp$ may be due to preferential alignment of the conducting channels in the plane of the film. It may also be due to errors in the two-probe method due to factors such as the coincidence of the current path and voltage sensing paths, and surface effects.

The equilibrated values of $\sigma_\parallel$ and $\sigma_\perp$ of aligned P3(21) samples are shown in Figure 7. In each case, we studied three independently prepared samples and the error bars represent the standard deviation of each data set. It is worth noting that $\sigma_\parallel/\sigma_\perp$ = 1.8 for the as-cast sample, a value that is significantly closer to unity than previous studies on nominally isotropic samples.[15−23] Birefringence measurements (Figure 5b) show the presence of weak anisotropy in these samples. We thus have a morphological basis

for the conductivity anisotropy. It is not clear, however, that the slight alignment obtained during casting is the main cause of the measured anisotropic conductivity. The effect of alignment is most clearly seen in the pressed samples where $\sigma_{\parallel}/\sigma_{\perp} = 75$. In spite of this, the relative increase in conductivity is modest; $\sigma_{\parallel}$ increases from 4.6×10^{-2} to 6.0×10^{-2} S/cm due to pressing. This implies that $\sigma_{\parallel}/\sigma_{iso}$ is 1.3, which is not very different from the predicted value of 1.5 (see Introduction). The difference between 1.3 and 1.5 may be due to alignment imperfections or nonrandom domain alignment in the as-cast films.

While the morphological data give in Figures 4 and 6 clearly demonstrate the presence of perpendicularly aligned lamellae, the conductivity data remain unaffected by this alignment, as shown in Figure 7. The value of $\sigma_{\perp}$ from the E-field and shear flow samples, 2.8×10^{-2} and 3.1×10^{-2}, respectively, are somewhat higher than that of the as-cast sample, 2.5×10^{-2} S/cm. The value of $\sigma_{\parallel}$ from the E-field sample of 3.6×10^{-2} S/cm is lower than that of the as-cast sample, 4.5×10^{-2} S/cm. However, the value of $\sigma_{\parallel}$ from the flow aligned sample, a protocol that led to much better alignment than the E-field protocol, is within experimental error of that of the as-cast sample. Even more troubling is the observation that for both E-field aligned and flow aligned samples, $\sigma_{\parallel} > \sigma_{\perp}$. We conclude that although our application of E-fields and flow fields results in significant alignment of the lamellae, the net effect of this on $\sigma_{\perp}$ and anisotropic conduction is not significant. This is because conductivity requires connectivity of microdomains across macroscopic length scales and obtaining this in the perpendicular orientation appears difficult. Some of the difficulties described here may be arising from the lack of information on impedances at the electrode−electrolyte interfaces.

Conclusions

The effect of lamellar alignment on conductivity in films of a poly(styrenesulfonate-*b*-methylbutylene) (PSS−PMB) copolymer was studied by impedance spectroscopy. Solvent casting results in a nearly isotropic sample composed of randomly orientated grains. Pressing the sample results in lamellae aligned in the plane of the film. Application of E-fields and flow fields results in lamellae aligned perpendicular to the plane of the film. The alignment obtained from the flow field was significantly better than that obtained from the E-field. The alignment of lamellae was quantified by a combination of 2D SAXS, birefringence, and TEM. Quantitative relationships between domain orientations and transport properties were obtained by carrying out in-plane and normal-to-plane proton conductivity measurements of aligned samples. Only the pressed sample showed highly anisotropic proton conduction with $\sigma_{\parallel}/\sigma_{\perp} = 75$. In this case, the value of $\sigma_{\parallel}$ increased by 30% after alignment, relative to that obtained from the as-cast samples. The values of $\sigma_{\parallel}/\sigma_{\perp}$ obtained from after E-field and shear flow alignment of 1.3 and 1.4, respectively, were lower than that of the nearly isotropic, as-cast membrane with $\sigma_{\parallel}/\sigma_{\perp} = 1.8$. However, the increase in $\sigma_{\perp}$ after alignment was less than 20%.

For practical applications, $\sigma_{\perp}$ is the quantity of prime importance. While it may be possible to increase $\sigma_{\perp}$ by alignment, our results suggest that the expected increase in conductivity will equal to or less than a factor of 1.5 for lamellar domains. While alignment of self-assembled microdomains has been studied extensively,[15−23,35−41] our knowledge of the connectivity across slightly misaligned microdomains is not well-developed. Our work thus far suggests that the measured conductivity of samples with perpendicular alignment is dominated by the lack of connectivity across slightly misaligned microdomains rather than microdomain alignment. Given these difficulties, it may be prudent to pursue other methods for improving $\sigma_{\perp}$ of PEMs in the near future.

Acknowledgment. Prof. M. J. Park acknowledges the POSTECH Basic Science Research Institute Grant and WCU (World Class University) program through the Korea Science and Engineering Foundation funded by the Ministry of Education, Science and Technology (Project No. R31-2008-000-10059-0). Prof. N. P. Balsara acknowledges the Electron Microscopy of Soft Matter Program at Lawrence Berkeley National Laboratory (LBNL) supported by the Director, Office of Science, Office of Basic Energy Sciences, Materials Sciences and Engineering Division, of the U.S. Department of Energy under Contract No. DE-AC02-05CH11231. TEM was performed at the National Center for Electron Microscopy at LBNL. SAXS measurements were conducted on the beamline 7.3.3 instrument at the ALS (LBNL).

References and Notes

(1) Hickner, M. A.; Ghassemi, H.; Kim, Y. S.; Einsla, B. R.; McGrath, J. E. *Chem. Rev.* **2004**, *104*, 4587–4611.
(2) Mauritz, K. A.; Moore, R. B. *Chem. Rev.* **2004**, *104*, 4535–4585.
(3) Kreuer, K. D. In *Handbook of Fuel Cell−Fundamentals, Technology and Applications*; Vielstich, W., Lamm, A., Gasteiger, H. A., Eds.; John Wiley & Sons Ltd.: Chichester, U.K., 2003; Vol. *3*, Part 3.
(4) Heitner-Wirguin, C. *J. Membr. Sci.* **1996**, *120*, 1–33.
(5) Ding, J. F.; Chuy, C.; Holdcroft, S. *Macromolecules* **2002**, *35*, 1348.
(6) Gao, J.; Lee, D.; Yang, Y.; Holdcroft, S.; Frisken, B. J. *Macromolecules* **2005**, *38*, 5854–5856.
(7) Rubatat, L.; Rollet, A. L.; Gebel, G.; Diat, O. *Macromolecules* **2002**, *35*, 4050.
(8) Yamada, M.; Li, D.; Honma, I.; Zhou, H. *J. Am. Chem. Soc.* **2005**, *127*, 13092–13093.
(9) Li, H.; Nogami, M. *Adv. Mater.* **2002**, *14*, 912–914.
(10) Marschall, R.; Rathouský, J.; Wark, M. *Chem. Mater.* **2007**, *19*, 6401–6407.
(11) Sasajima, K.; Munakata, H.; Kanamura, K. *J. Electrochem. Soc.* **2008**, *155*, B143–B147.
(12) Kinning, D. J.; Thomas, E. L.; Ottino, J. M. *Macromolecules* **1987**, *20*, 1129.
(13) Singh, M.; Odusanya, O.; Wilmes, G. M.; Eitouni, H. B.; Gomez, E. D.; Patel, A. J.; Chen, V. L.; Park, M. J.; Fragouli, P.; Iatrou, H.; Hadjichristidis, N.; Cookson, D.; Balsara, N. P. *Macromolecules* **2007**, *40*, 4578.
(14) Panday, A.; Mullin, S.; Gomez, E. D.; Wanakule, N.; Chen, V. L.; Hexemer, A.; Pople, J.; Balsara, N. P. *Macromolecules* **2009**, *42*, 4632.
(15) Elabd, Y. A.; Walker, C. W.; Beyer, F. L. *J. Membr. Sci.* **2004**, *231*, 181–188.
(16) Gardner, C. L.; Anantaraman, A. V. *J. Electroanal. Chem.* **1995**, *395*, 67.
(17) Pourcelly, G.; Oikonomou, A.; Gavach, C.; Hurwitz, H. D. *J. Electroanal. Chem.* **1990**, *287*, 43.
(18) Li, J.; Wilmsmeyer, K. G.; Madsen, L. A. *Macromolecules* **2009**, *42*, 255.
(19) Ma, S.; Siroma, Z.; Tanaka, H. *J. Electrochem. Soc.* **2006**, *153*, A2274.
(20) Cable, K. M.; Mauritz, K. A.; Moore, R. B. *Chem. Mater.* **1995**, *7*, 1601.
(21) Maki-Ontto, R.; de Moel, K.; Polushkin, E.; Alberda van Ekenstein, G.; ten Brinke, G.; Ikkala, O. *Adv. Mater.* **2002**, *14*, 357–361.
(22) Kato, T.; Mizoshita, N.; Kishimoto, K. *Angew. Chem., Int. Ed.* **2006**, *45*, 38–68.
(23) Liu, D.; Hickner, M. A.; Case, S. W.; Lesko, J. J. *J. Eng. Mater. Technol.* **2006**, *128*, 503.
(24) Umeda, M.; Uchida, I. *Langmuir* **2006**, *22*, 4476–4479.
(25) Li, J.; Kamata, K.; Komura, M.; Yamada, T.; Yoshida, H.; Iyoda, T. *Macromolecules* **2007**, *40*, 8125.
(26) Chen, H.; Palmese, G. R.; Elabd, Y. A. *Chem. Mater.* **2006**, *18*, 4875.
(27) Park, M. J.; Downing, K. H.; Jackson, A.; Gomez, E. D.; Minor, A. M.; Cookson, D.; Weber, A. Z.; Balsara, N. P. *Nano Lett.* **2007**, *7*, 3547.
(28) Park, M. J.; Nedoma, A. J.; Geissler, P. L.; Jackson, A.; Cookson, D.; Balsara, N. P. *Macromolecules* **2008**, *41*, 2271.
(29) Park, M. J.; Balsara, N. P. *Macromolecules* **2008**, *41*, 3678.
(30) Park, M. J.; Balsara, N. P. *Macromolecules* **2009**, *42*, 6808.
(31) Park, M. J.; Kim, S.; Minor, A. M.; Balsara, N. P. *Adv. Mater.* **2009**, *21*, 203.

(32) Beck Tan, N. C.; Liu, X.; Briber, R. M.; Peiffer, D. G. *Polymer* **1995**, *36*, 1969.
(33) Garetz, B. A.; Newstein, M. C.; Dai, H. J.; Jonnalagadda, S. V.; Balsara, N. P. *Macromolecules* **1993**, *26*, 3151.
(34) Wang, H.; Newstein, M. C.; Chang, M. Y.; Balsara, N. P.; Garetz, B. A. *Macromolecules* **2000**, *33*, 3719.
(35) Koppi, K. A.; Tirrell, M.; Bates, F. S.; Almdal, K.; Colby, R. H. *J. Phys. II France* **1992**, *2*, 1941.
(36) Hadziioannou, G.; Skoulios, A. *Macromolecules* **1982**, *15*, 258.
(37) Amundson, K.; Helfand, E.; Davis, D. D.; Quan, X.; Patel, S. S.; Smith, S. D. *Macromolecules* **1991**, *24*, 6546.
(38) Amundson, K.; Helfand, E.; Quan, X.; Smith, S. D. *Macromolecules* **1993**, *26*, 2698.
(39) Amundson, K.; Helfand, E.; Quan, X. N.; Hudson, S. D.; Smith, S. D. *Macromolecules* **1994**, *27*, 6559.
(40) Thurn-Albrecht, T.; DeRouchey, J.; Russell, T. P.; Jaeger, H. M. *Macromolecules* **2000**, *33*, 3250.
(41) Goulian, M.; Milner, S. T. *Phys. Rev. Lett.* **1995**, *74*, 1775.
(42) Patel, S. S.; Larson, R.; Winey, K. I.; Watanabe, H. *Macromolecules* **1995**, *28*, 4313.
(43) Gupta, V. K.; Krishnamoorti, R.; Kornfield, J. A.; Smith, S. D. *Macromolecules* **1995**, *28*, 4464.
(44) Zhang, Y.; Weisner, U.; Yang, Y.; Pakula, T.; Speiss, H. W. *Macromolecules* **1996**, *29*, 5427.
(45) Balsara, N. P.; Hammouda, B. *Phys. Rev. Lett.* **1994**, *72*, 360.
(46) Hahn, H.; Lee, J. H.; Balsara, N. P.; Garetz, B. A.; Watanabe, H. *Macromolecules* **2001**, *34*, 8701.
(47) Graessley, W. W. Viscoelasticity and Flow in Polymer Melts and Concentrated Solutions. In *Physical Properties of Polymers*, 2nd ed.; American Chemical Society: Washington, DC, 1993.
(48) Born, M.; Wolf, E. In *Principles of Optics: Electromagnetic Theory of Propagation, Interference and Diffraction of Light*, 6th ed.; Cambridge University Press: New York, 1997.
(49) Elabd, Y. A.; Napadensky, E.; Walker, C. W.; Winey, K. I. *Macromolecules* **2006**, *39*, 399–407.
(50) Sirringhaus, H.; Brown, P. J.; Friend, R. H.; Nielen, M. M.; Bechgarrd, K.; Langeveld-Voss, B. M. W.; Spiering, A. J. H.; Janssen, R. A. J.; Meijer, E. W.; Herwig, P.; de Leeuw, D. M. *Nature* **1999**, *401*, 685.
(51) Xu, Y.; Gu, W.; Gin, D. L. *J. Am. Chem. Soc.* **2004**, *126*, 1616–1617.